ADVANCED FUNCTIONAL MATERIALS
www.afm-journal.de

On-Chip Self-Assembly of a Smart Hybrid Nanocomposite for Antitumoral Applications

Bárbara Herranz-Blanco, Dongfei Liu, Ermei Mäkilä, Mohammad-Ali Shahbazi, Eloy Ginestar, Hongbo Zhang, Vladimir Aseyev, Vimalkumar Balasubramanian, Jarno Salonen, Jouni Hirvonen, and Hélder A. Santos**

A hybrid nanocomposite comprised by porous silicon nanoparticles and a stimuli responsive polymeric material, polyethylene glycol-block-poly(L-histidine), is spontaneously formed by nanoprecipitation in a flow-focusing microfluidic chip. The nanocomposite presents a novel hybrid compound micelle structure with a great robustness for therapeutic applications. Therefore, the nanocomposite is developed and tested as a "smart" multistage drug delivery system (MDDS) in response to some of the current problems that cancer treatment presents. Based on the stimuli-responsive behavior of the nanocomposite, a chemotherapeutic agent is successfully loaded into the nanosystem and released upon changes in the pH-values. The nanocomposite demonstrates enhanced stability in plasma, narrow size distribution, improved surface smoothness, and high cytocompatibility. Furthermore, the nanocomposite presents reduced nanoparticle internalization by phagocytic macrophage cells and pH-dependent cell growth inhibition capacity. Overall, the developed hybrid nanocomposite shows very promising features for its further development as a "smart" pH-responsive MDDS.

1. Introduction

Cancer treatment still remains a challenge, greatly due to the lack of tumor-specificity of the anticancer drugs that lead to undesirable side effects and loss of therapeutic efficiency. In addition, chemotherapeutics are usually poorly water-soluble compounds, making their formulation rather challenging. Accordingly, in the past decades, drug delivery systems have been developed to solve several of these problems and improve the therapeutic effect of chemotherapeutics.[1]

Mesoporous silicon nanoparticles (PSi NPs) are an example of a promising drug delivery system.[2] Their mesopores (2–50 nm) allow the loading of drugs by simple physical adsorption or electrostatic interactions, keeping the molecules loaded inside the mesopores in their amorphous-like state, which drastically increases their solubility,[3] providing the PSi NPs with the capacity to fulfill a key prerequisite for the formulation of chemotherapeutics. Other attractive properties of the PSi NPs include large surface area and pore volume, high drug-loading degree, biocompatibility, and biodegradability.[4] Nevertheless, PSi NPs also have certain limitations. For example, fast and undesirably premature drug release caused by metabolites and ions in the body fluids that can rapidly displace the cargos loaded in the freely accessible mesopores.[5]

On the other hand, amphiphilic copolymers composed of polyethylene glycol (PEG) and biodegradable poly(aminoacids) may also be utilized as drug nanocarriers because of their versatility and biocompatibility,[6] such as polyethylene glycol-block-poly(L-histidine) (PEG-b-PHIS) and poly(ethylene glycol)-block-polylactide methyl ether (PEG-b-PLA) (Figure S1, Supporting Information). PEG-b-PHIS exhibits a pH-responsive behavior due to the presence of a protonable nitrogen on its imidazole ring. In solution, when the polymer is not protonated it tends to self-assemble, driven by the attractive hydrophobic forces to form supramolecular structures.[7] However, when the copolymer is protonated the positive charges exert repulsive forces in opposition to the hydrophobic ones and the polymers are not able to self-assemble. In addition, PEG-b-PLA in combination with the pH-sensitive polymer (PEG-b-PHIS) forms a mixed supramolecular structure. PEG-b-PLA molecules work reinforcing the hydrophobic interactions between the molecules, thus tuning the pH-value at which conformational changes occur proportionally to the

B. Herranz-Blanco, Dr. D. Liu, E. Mäkilä, M.-A. Shahbazi, E. Ginestar, Dr. H. Zhang, Dr. V. Balasubramanian, Prof. J. Hirvonen, Prof. H. A. Santos
Division of Pharmaceutical Chemistry and Technology
Faculty of Pharmacy
University of Helsinki
FI-00014 Helsinki, Finland
E-mail: barbara.herranz@helsinki.fi; helder.santos@helsinki.fi
E. Mäkilä, Prof. J. Salonen
Laboratory of Industrial Physics
Department of Physics
University of Turku
FI-20014 Turku, Finland
Dr. H. Zhang
School of Engineering and Applied Sciences
Harvard University
Cambridge, MA 02138, USA
Dr. V. Aseyev
Laboratory of Polymer Chemistry
Department of Chemistry
University of Helsinki
FI-00014, Helsinki, Finland

DOI: 10.1002/adfm.201404122

concentration of these molecules.[8] As a result of the self-assembly of the copolymers, a drug in solution could also be entrapped within the nanostructure and triggered released upon pH destabilization. However, the hydrophobic molecules can hinder the use of this biomaterial because of their slow dissolution rate.

To overcome some of the issues that cancer treatment still presents, herein we propose the design of a smart hybrid nanocomposite, a multistage drug delivery system (MDDS) comprised of PSi NPs as the first-stage drug nanocarrier and the second-stage being the pH-sensitive polymeric structure assembled on top of the NPs. The first stage can load a great variety of molecules and increase the dissolution rate of the poorly water-soluble drugs, whereas the second-stage can satisfy the characteristics that an ideal nanocarrier requires, i.e., biocompatibility, stability along the delivery route, increased circulation time by evading the mononuclear phagocyte system (MPS) detection, and thus, macrophage-mediated clearance as well as favorable characteristics for tumor enhanced permeability and retention (EPR).[9] In combination, both particle stages can render an advanced and versatile platform for the loading of multiple drugs, with stimuli-controlled release properties.

The hybrid nanocomposite was produced by microfluidic nanoprecipitation (**Figure 1**).[10] PSi NPs and the solubilized amphiphilic polymers were forced to coflow with a miscible antisolvent inside a flow-focusing glass capillary chip. Both fluids rapidly mixed causing nanoprecipitation and self-assembly of the copolymers with the PSi NPs forming the hybrid nanocomposite. This method presented the advantage of being fast, highly reproducible, and controllable by setting the flow rates at which the fluids are pumped inside the chip, achieving different mixing rates, and thus, different NPs' sizes.[10a]

Structurally, the selected copolymers, in association with the hydrophobic PSi NPs, resulted in the formation of a PSi/polymeric composite (PSi–PC) which was demonstrated to be a compound micelle assembled on the surface of the PSi NPs. Compound micelles have been described as aggregates of reverse micelles of amphiphilic block-copolymers, consisting on a hydrophilic core and a hydrophobic corona, stabilized by the presence of an amphiphilic polymeric layer with the hydrophilic block faced toward the surface.[11] The formation of reversed micelles was proved in the case of copolymers with a low ratio of hydrophilic-to-hydrophobic blocks. In our case, the ratio between the hydrophilic and hydrophobic blocks was variable, i.e., PEG-b-PHIS had a ratio of 1:1 to 1:5, because of the multiple chain lengths of the PHIS block (from 5 to 25 kDa); and PEG-b-PLA of 0.75:1. Therefore, the copolymers with the lower hydrophilic-to-hydrophobic ratio can form reverse micelles. In addition, the PSi NPs present in the suspension were hydrophobic. Therefore, in order to render the final hybrid nanocomposite, the copolymers in solution can interact through their hydrophobic blocks with the hydrophobic surface of the PSi NPs. Upon the nanoprecipitation process the reversed micelles can self-assemble on the surface of the previously formed structure, while the solvent and antisolvent are mixed. Finally, the system can be further stabilized in the aqueous medium by a layer of copolymers with their hydrophilic blocks, PEG, facing the outer medium (Figure 1). The final compound micelle, presented a packed and solid structure,[12] being a good candidate for developing a robust controlled drug delivery system. To the best of our knowledge, this is the first attempt to entrap PSi NPs through this approach.

In terms of design, the combination of the block copolymers was selected to suit tumor pH-conditions as the trigger for drug release (pH below 6.8).[7,13] In addition, the PEG corona formed on the surface of the particles can help to prolong the circulation time of the NPs in the bloodstream, promoting the EPR effect[14] and inhibiting the drug efflux pumps in cancer cells, a common mechanism observed in multidrug resistance.[15]

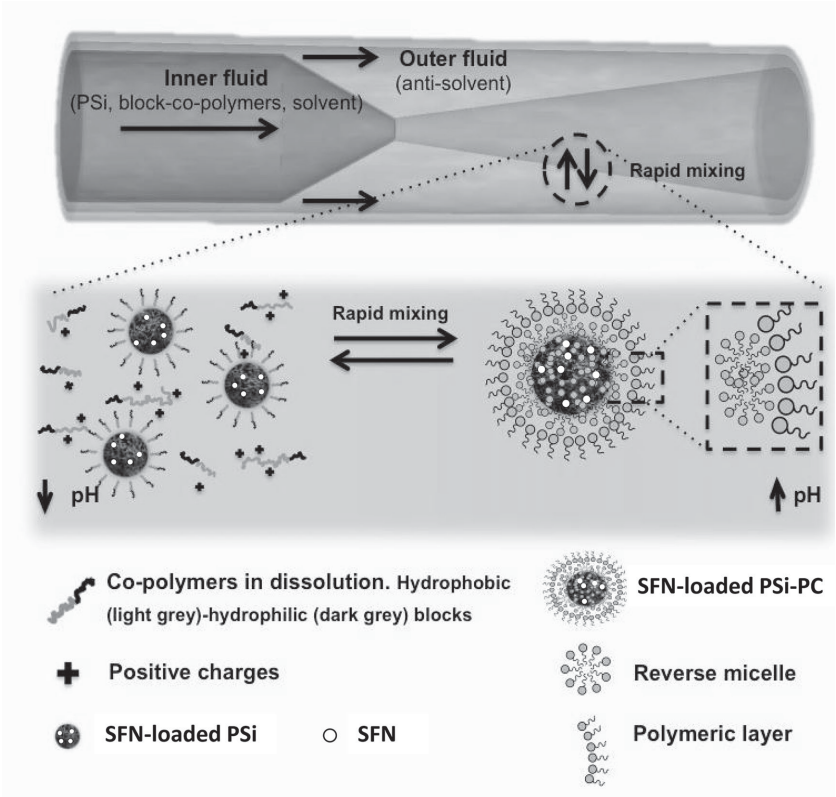

Figure 1. Schematic representation of the microfluidic nanoprecipitation process. The inner fluid carries the amphiphilic block-copolymers in solution and PSi NPs in suspension; the outer fluid serves as the antisolvent. Both the fluids coflow within the micrometric channels of the flow-focusing glass capillary device and rapidly mix causing the nanoprecipitation and self-assembly of the components to form the PSi–polymer composite (PS–PC). SFN abbreviation stands for anticancer drug sorafenib.

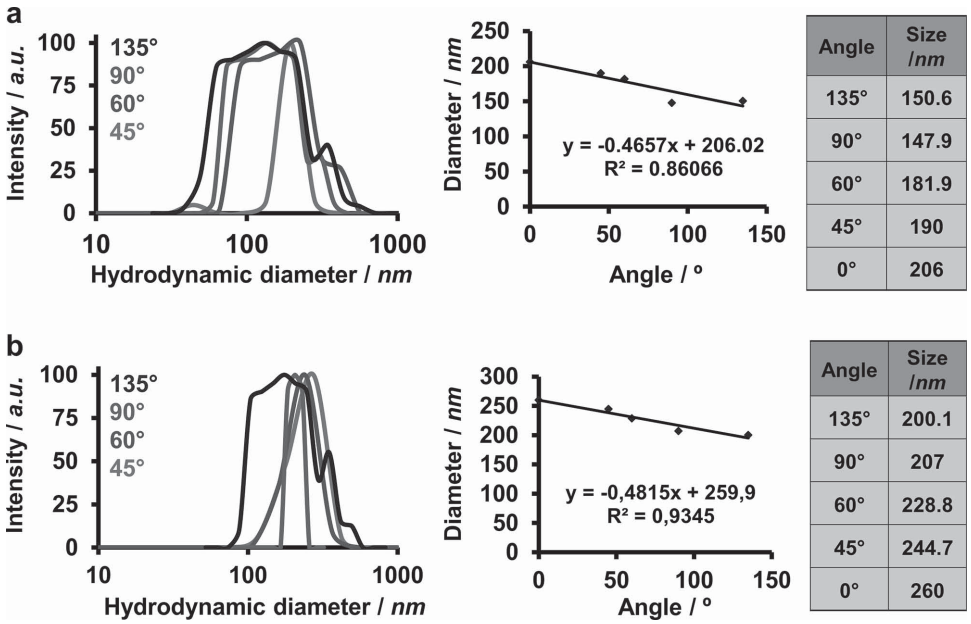

Angle	Size /nm
135°	150.6
90°	147.9
60°	181.9
45°	190
0°	206

Angle	Size /nm
135°	200.1
90°	207
60°	228.8
45°	244.7
0°	260

Figure 2. Size values obtained by multiangular DLS at different detection angles. a) Polymeric nanoparticles and b) PSi–PC. The final size was obtained by extrapolation at 0°.

2. Results and Discussion

2.1. Characterization of the PSi NPs and PSi–PC

The specific surface area of the plain PSi nanoparticles obtained from the adsorption isotherm was ≈213 ± 5 m^2 g^{-1}, the total pore volume was ≈0.75 cm g^{-1} (Figure S2, Supporting Information), and the calculated average pore size was ≈14.2 ± 0.3 nm.

PSi NPs and the produced PSi–polymer composite (PSi–PC) were characterized by attenuated total reflection Fourier transform infrared spectroscopy (ATR–FTIR), dynamic backlight scattering (DLS), multiangular DLS, and transmission and scanning electron microscopy (TEM and SEM) (**Figures 2** and **3**), in order to prove and study the micellar self-assembly on the surface of the PSi NPs. PEG-b-PHIS preparation was also confirmed by ^{1}H-NMR (Figure S3, Supporting Information).

The NPs size showed angular dependency, as a result of their moderate polydispersity and possible nonspherical shape of the PSi–PCs (Figure 2).[16] The empty compound micelles (without PSi) and the nanocomposites showed an average size

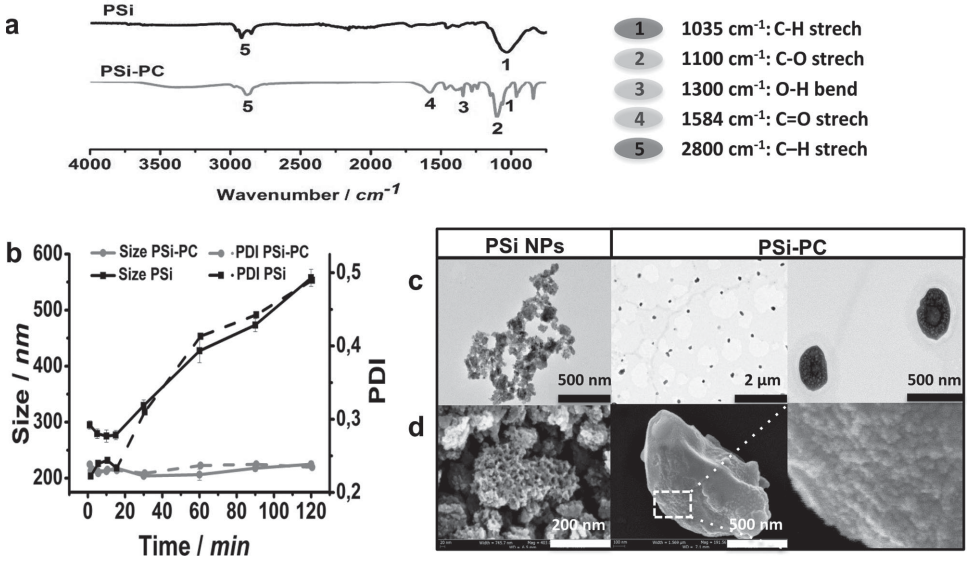

Figure 3. Characterization of the PSi NPs and PSi–PCs. a) ATR–FTIR spectra of PSi NPs and PSi–PCs. b) PSi NPs and PSi–PCs stability in plasma for 2 h measured with a detection angle of 173° (Zetasizer Nano). Solid lines represent the NPs' size and dashed lines the PDI. c) TEM and d) SEM images of the PSi–PCs and PSi NPs. PDI abbreviation stands for polydispersity index.

of 206 and 260 nm, respectively (Figure 2). Both values were calculated by extrapolation from the data obtained at different angles of detection to angle 0°. The polydispersity was in both cases below 0.2, representative of a homogeneous particle size distribution. Overall, these results suggest the embedment of the PSi NPs by the polymeric micellar formation, due to the increase in size of the PSi–PCs (260 nm) compared to the PSi NPs (≈130 nm). Moreover, the composites were well dispersed and highly stable without formation of particle aggregates, unlike the bare PSi NPs.

The surface zeta (ζ)-potential values of the PSi NPs and the PSi–PCs were −14.8 and −5 mV, respectively. The empty polymeric micelles (without PSi NPs) were also analyzed for comparison, presenting a surface ζ-potential of +2.8 mV. Thus, the negative surface ζ-potential of the PSi NPs appeared to be compensated by their interaction with the polymeric micelles (+2.8 mV), showing a composite with a final surface ζ-potential significantly less negative than its bare counterpart.

ATR–FTIR was used for the determination of the chemical groups presented on the surface of the PSi NPs and PSi–PCs. (Figure 3a). The clear attenuation of the peaks coming from PSi after the microfluidic nanoprecipitation and the appearance of representative peaks corresponding to the polymers used in the formation of the nanocomposites (Figures S4 and S5, Supporting Information), suggested a comprehensive formation of the micellar assembly on the surface of the PSi NPs.

Furthermore, the structure of the PSi–PCs was characterized by TEM (Figure 3c) and SEM (Figure 3d). The PSi NPs presented an irregular shape, with a porous structure and rough surface,[17] whereas the PSi–PCs presented a more regular shape and smoother surface, without observable pores. The surface-forming micelles were further confirmed by SEM imaging. Moreover, the bare PSi NPs were not found in any of the PSi–PCs' samples imaged by TEM and SEM.

2.2. Stability of the Nanocarriers in Human Plasma

Next, we investigated the stability of the PSi–PCs in physiological conditions (Figure 3b). The physiological stability of NPs is related to the plasma protein corona formation, which is crucial to predict the fate of the NPs in vivo.[18] In the protein corona formation, opsonins have an important role, driving the activation of NPs' recognition by the immune cells and their fast clearance from the blood circulation. Protein corona formation can be detected by an increase in the NPs' size when exposed to human plasma.[18c] Accordingly, we measured the size of the bare PSi NPs and the PSi–PCs after being stirred in plasma at 37 °C for up to 2 h. The PSi NPs abruptly increased their size from ≈130 to 300 nm and further to 550 nm within 120 min. whereas the size of the PSi–PCs remained unchanged along the study at ≈215 nm. The polydispersity followed the same pattern as the size of the NPs. Notably, it can be observed a difference between the NPs' size measured previously in Milli-Q water and in human plasma. This difference is due to the different techniques used for size analysis. In the first case, the size was measured by multiangular light scattering, and the given size value was calculated by extrapolation (see Section 2.1 and Figure 2), whereas in the latter case the size was measured using the ZetaSizer Nano instrument, having a detection angle fixed at 173°.

Overall, the produced PSi–PCs showed improved stability in simulated physiological conditions compared to the PSi NPs, suggesting the lesser extent of protein corona formation around PSi–PC NPs compared to PSi NPs.[18c] This fact could be determinant for a favorable biodistribution and reduced blood clearance of the nanocomposites in vivo.[18]

2.3. Particle Size and ζ-potential at Different pH-Values

The key feature of the PSi–PCs was its capacity to respond to pH changes, which was evaluated by changes in the particle size, surface ζ-potential, and also by TEM imaging (**Figure 4**). Figure 4a and Figure S6 (Supporting Information) show the pH-values versus PSi–PC's size and surface ζ-potential. The average nanoparticle size was increased when the pH was decreased from 7.4 to 5.5, and dramatically decreased at pH 3. The surface ζ-potential changed from −6 to +7 mV as the pH decreased. We propose that upon the pH decrease from 7.4 to 3, the pH-sensitive polymer, which presents a poly-L-histidine block with a protonable nitrogen on its imidazole ring, gradually protonated and increased the repulsive forces among the chains of the polymer, forming a less tightly packed structure, which eventually led to the total disruption of the nanocomposite and release of the PSi NPs.[19]

TEM images were also used to further confirm the progressive pH-dependent disruption of the PSi–PC matrix (Figure 4b). At pH 7.4, the structure of the composite was packed, whereas at pH 5.5 an incipient disassembling of the polymeric micelle was reflected, exposing in some cases the PSi NPs to the external environment.

The NP size increment taking place below 7.4, besides allowing a pH-controlled drug delivery, it could also serve as a one-way trafficking tool for the nanocomposites, reinforcing the physiological enhanced retention effect present in tumors.

2.4. Drug Loading and pH-dependent Drug Release

The PSi–PC's capacity to control drug release in response to changes in the pH was also evaluated. In this respect, sorafenib (SFN), a cytotoxic drug that inhibits cell proliferation and angiogenesis, was used as a model drug. SFN-loaded PSi NPs were used to produce SFN-loaded PSi–PCs. For both types of particles, the drug loading degree (LD) was determined by completely releasing their cargo and analyzing it by high performance liquid chromatography (HPLC). The obtained LD of SFN on PSi NPs was 5.8% and the loading efficiency of the drug on the nanocomposites was 4.9%. Subsequently, we studied the release of SFN from the SFN-loaded NPs under different conditions. To mimic the physiological tumoral microenvironment and the intracellular conditions, we used human plasma (pH 7.4) and phosphate buffered saline enriched with 10% heat inactivated fetal bovine serum (PBS–FBS) with a pH of 6.8 and 5.5, respectively. Due to the aqueous insolubility of SFN, FBS had to be used to allow the release of the drug.[2d] The drug release profiles are shown in Figure 4c. Pure SFN

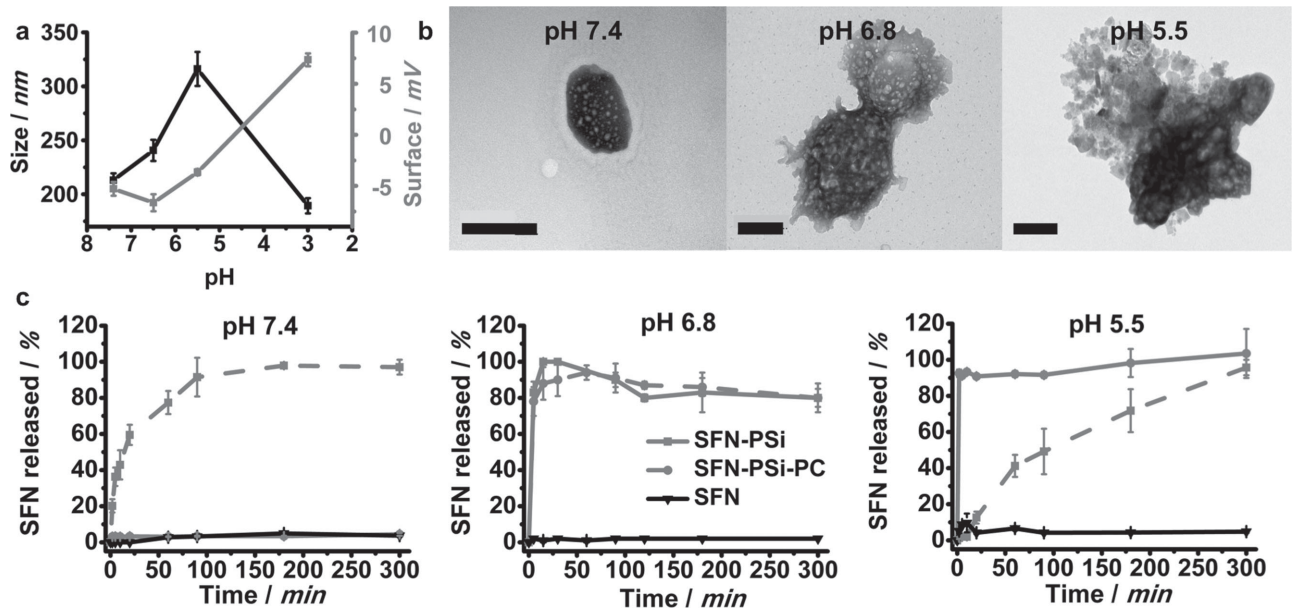

Figure 4. The pH-dependent changes of the PSi–PCs and its influence on drug release. a) Average size (black; left axis) and surface ζ-potential (gray; right axis) are represented against pH-values. b) TEM images showing the PSi–PCs after being suspended in Milli-Q water at different pH-values. The scale represents 200 nm. c) Drug release profiles at pH 7.4 (left), 6.8 (middle), and 5.5 (right). Pure SFN (black solid line), SFN-loaded PSi (gray dashed line), and SFN-loaded PSi–PC (gray solid line) are shown. Errors bars represent the mean ± s.d. ($n = 3$).

in solution was only detected in all the media below 10%, due to the remarkably low solubility of SFN. However, SFN-loaded PSi greatly improved the drug's release up to ≈100%. Interestingly, SFN release from the PSi–PC in plasma at pH 7.4 was low (<5%), whereas in PBS–FBS at pH 6.8 and 5.5 a burst-type release profile was observed. This pH-dependent behavior of the nanocomposites could be explained by the protonation of the pH-responsive copolymer when exposed to mild acidic media, increasing the repulsive forces among the chains of the polymer to render a less tightly packed structure, and eventually leading to the total disruption of the nanocomposite and release of the PSi NPs and of the cargo loaded within the PSi NPs.[19]

These experiments confirmed the potential of PSi to significantly increase the dissolution rate of SFN, and further highlighted the robustness of the nanocomposite to protect the drug inside the nanostructure, preventing any leakage at physiological conditions (pH 7.4).

2.5. In Vitro Cytotoxicity

As a result of the promising pH-triggered MDDS produced, we further assessed its safety (cytotoxicity) (**Figure 5**), its capacity to evade the MPS' recognition, and its ability to inhibit the growth of cancer cells (**Figure 6**). To test the cytotoxicity and growth inhibition, PC3MM2 cells derived from human prostate cancer were used. The cytotoxicity was assessed for PSi NPs and PSi–PCs without the drug, whereas to determine their cell growth inhibition potential SFN-loaded NPs were tested. The in vitro cytotoxicity (Figure 5a) performed at pH 7.4 showed that the PSi NPs and PSi–PCs were not significantly toxic below the concentration of 0.1 mg mL^{-1}. In addition, the PSi–PCs were 20% less toxic than the PSi NPs at the concentration of 0.25 mg mL^{-1}. At pH 5.5, the PSi–PC was significantly less toxic than the PSi NPs up to 0.5 mg mL^{-1}. Doses of 0.25 and 0.5 mg mL^{-1} of PSi–PC at both pH-values of 5.5 and 7.4, respectively, allowed a survival rate of the PC3MM2 cells of at least 80%.

The relatively low cytotoxicity of the nanocomposites could be ascribed to the presence of biocompatible polymers on their surface,[6] and moreover, to the exposure of the hydrophilic PEG block. The interaction of hydrophilic NPs with the cells' membranes is weak, mediated by water molecules, which make the particle–cell interactions less likely to occur,[20,21] thus increasing the cytocompatibility of the NPs.

2.6. Cancer Cell Growth Inhibition

The cell growth inhibition was tested for the SFN-loaded nanocarriers under standard cell culturing conditions (pH 7.4) and under modified pH 5.5 conditions. Since drug release has been demonstrated to occur at both pH 6.8 and 5.5, the lowest pH value (5.5) was chosen as a way to compare the effect of the drug loaded nanocomposites under healthy physiological conditions, where drug release is not expected; its effect under acidic conditions, found in the extracellular tumor microenvironment or intracellular endosomes, where SFN has proved to be released from the nanocomposites and could therefore exert its effect on the cancer cells. The results were expressed in terms of SFN concentration (μM) (Figure 5b). Pure SFN at both pH-values tested showed an IC_{50} below 15×10^{-6} M. SFN-loaded PSi NPs presented an IC_{50} of $\approx 27 \times 10^{-6}$ M at pH 7.4 $\times 10^{-6}$ M and

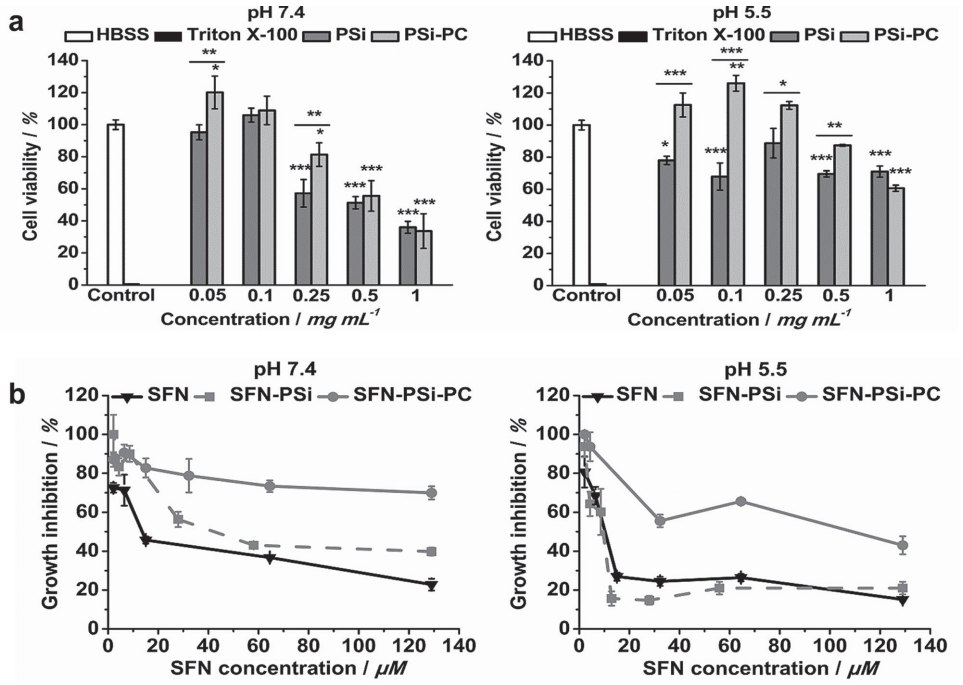

Figure 5. In vitro cell experiments. a) Cytotoxicity assessment of the PSi NPs and PSi–PCs. The PC3MM2 prostate cancer cells were incubated for 24 h with the NPs at pH 7.4 and 5.5. b) SFN-loaded PSi NPs and PSi–PCs cell growth inhibition evaluation. The drug-loaded NPs were incubated for 24 h with PC3MM2 cells at pH 7.4 and 5.5. Errors bars represent the mean ± s.d. ($n = 3$). HBSS abbreviation stands for Hank's balanced Salt solution. HBSS and Triton X-100 were used as controls.

8×10^{-6} M at pH 5.5. SFN-loaded PSi–PC showed a half maximal inhibitory concentration (IC_{50})around 32×10^{-6} M at pH 5.5. However, at pH 7.4, the IC_{50} was not reached within the concentration range tested (130×10^{-6} M). Moreover, the greatest cell growth inhibition exerted by the SFN-loaded PSi–PCs at pH 7.4 was 30% lower than the bare SFN-loaded PSi and 43% lower than the pure drug.

According to these results, the SFN-loaded PSi–PC demonstrated to be an effective protection for the premature release of SFN from the mesopores of PSi NPs and its effects toward PC3MM2 cells under simulated physiological conditions (pH 7.4). However, even though the drug loaded nanocomposites showed a greater toxic effect under acidic conditions compared to physiological conditions, their effect was not as strong as the observed for the free drug. Therefore, to really assess the superiority of the nanocomposites, the output of the combination of pH triggered drug release and passive targeted delivery should be studied in vivo.

2.7. In Vitro Macrophage-Mediated Phagocytosis of PSi and PSi–PC

A further benefit of the PSi–PCs is the presence of PEG on its surface, which has been demonstrated to reduce the NPs detection by the MPS, thus prolonging the NPs' circulation time in the bloodstream.[14] We also carried out an in vitro macrophage-mediated phagocytosis test with both PSi NPs and PSi–PC using RAW 264.7 macrophage cells. The NP–cell interactions were evaluated by confocal microscopy and flow cytometry. As shown in Figure 6a, tetramethylrhodamine (TRITC)-labeled PSi NPs exhibited a greater fluorescence density inside the space delimited by the fluorescently labeled membrane of the macrophages compared with the TRITC-labeled PSi–PCs, indicating that the PSi NPs were more likely to be phagocytized than the PSi–PCs. These images were quantitatively supported by the flow cytometry results (Figure 6b). The results showed a percentage of positive events for the PSi NPs and PSi–PCs as of 93.5% and 24%, respectively, corroborating that the macrophages had less tendency to interact with the PSi–PCs than with bare PSi NPs, most likely due to the presence of a PEG (5 kDa) corona on the surface of the nanocomposites. This molecule has shown a great reduction in plasma protein absorption, including opsonins that mediate clearance by the cells of the MPS,[22] leading to the lesser extent of the NPs uptake.

3. Conclusion

In conclusion, we have presented a smart hybrid nanocomposite consisting of a pH-sensitive polymeric compound micelle assembled on the surface of PSi NPs (PSi–PCs) produced by flow-focusing microfluidic nanoprecipitation. PSi–PC was further investigated due to its potential as a MDDS. The produced nanocomposites showed a narrow size distribution and surface smoothness compared to its bare counterpart. Moreover, PSi–PCs showed enhanced plasma stability and an adequate size for EPR effect. A chemotherapeutic agent (SFN) was successfully loaded on the MDDS, and protected from the external simulated physiological conditions (pH 7.4).

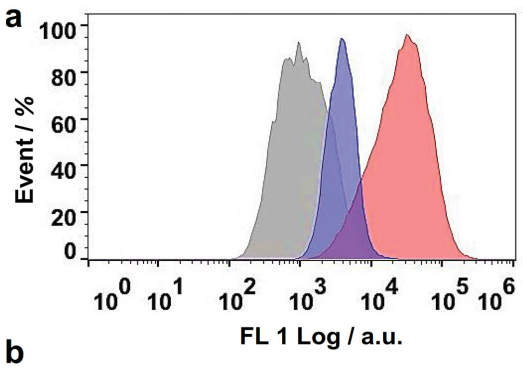

Sample	MFI / a.u.	Positive events / %
RAW 264.7 (-)Control	6084	0
RAW 264.7 / PSi-PC	6583	24
RAW 264.7 / PSi NPs	27673	93.5

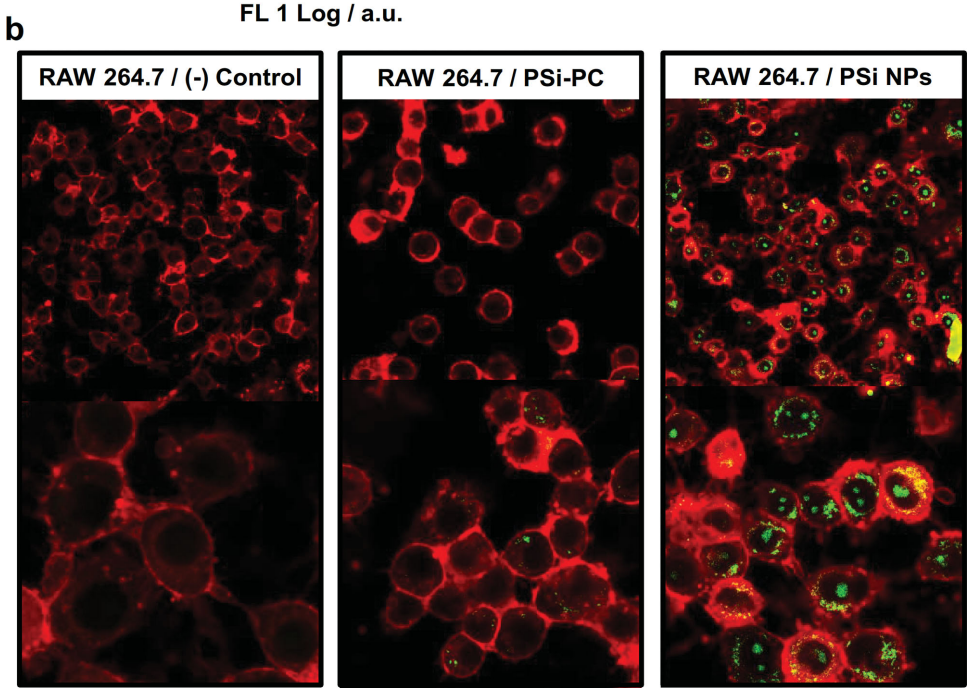

Figure 6. Evaluation of macrophage-mediated NPs' (PSi and PSi–PC) phagocytosis after 3 h incubation of the NPs with RAW 264.7 macrophages. a) Qualitative cell–NP localization by confocal microscopy. The PSi NPs were labeled with tetramethylrhodamine (TRITC) and the cells' membrane with CellMask Deep Red (Life Technologies, USA). A negative control (cells without any treatment) and two positive controls (TRITC-labeled PSi NPs and TRITC-labeled PSi–PC) are shown. The colors of the fluorescence emission signal were modified for a clearer visualization. TRITC is shown in green and CellMask Deep Red in red. b) Quantitative analysis by flow cytometry. The PSi NPs were labeled with Alexa Fluor 488. The graph represents the % of positive events against their fluorescence intensity. The gray curve represents the negative control (cells without any treatment), the blue curve represents the cells incubated with Alexa Fluor 488-labeled PSi–PC, and the red curve represents the cells incubated with Alexa Fluor 488-labeled PSi. The table summarizes the mean fluorescence intensity and the %-positive events for each sample.

Conversely, the smart polymeric system allowed fast release of the payload under simulated acidic tumoral and intracellular conditions. Accordingly, the SFN-loaded PSi–PC evidenced a pH-dependent cell growth inhibition capacity in a prostate cancer cell line, resulting in more cell death at pH 5.5 than at pH 7.4. This demonstrates the potential of the developed nanocomposite to reduce drugs' unspecific effect over healthy tissues and to increase the treatment's specificity and efficiency. Furthermore, the nanocomposite presented high cytocompatability and capacity to minimize the interactions with macrophage cells, which can be indicative of the potential of the composite to increase its blood circulation time, and thus, reduce its body clearance. Overall, the PSi–PC MDDS has proved to be a good candidate for further development as a platform for cancer drug delivery.

4. Experimental Section

Synthesis of Poly(Ethylene Glycol)-Block-Poly(L-Histidine): The synthesis of the block-copolymer of poly(L-histidine) (5–25 kDa; Figure S1, Supporting Information) was performed as described in ref.[22a] Briefly, the block-copolymer was dissolved in 10×10^{-3} M acetic acid (5 mL), then the pH was adjusted to 6.5 by adding 0.1 M sodium hydroxide. Afterwards, N-hydroxylsuccinimide (NHS) functionalized PEG (mPEG-NHS; 5 kDa) was added to the solution in excess, in a of 1.2:1 (mol:mol). The polymers were let to react in a round-bottom flask for 8 h under nitrogen gas flux. The product, PEG-PHIS (Figure S1, Supporting Information), was purified for 72 h by dialysis against deionized water using a cellulose ester membrane (8–10 kDa). The purified block-co-polymer was then lyophilized. To prove the successful synthesis of PEG-PHIS, the final product was analyzed by ^{1}H-NMR (Figure S3, Supporting Information), and ATR–FTIR (Figures S4 and S5, Supporting Information). Moreover, the yield of the reaction was calculated to be of 79%.

Production of PSi and PSi–PC: Fabrication of the PSi NPs is described in detail in refs.[4b,23] PSi–PC was produced by on-chip nanoprecipitation. The inner fluid was prepared by mixing the PSi NPs with the polymers in solution. PEG-b-PLA (62.5 μg) was dissolved in 750 mL of ethanol, and PEG-b-PHIS (187.5 μg) in 0.1 M hydrochloric acid (250 μL) containing 0.3×10^{-3} M of citric acid and 0.2% of surfactant F127. PSi was added to the PEG-b-PHIS solution and dispersed by sonication. Then it was mixed with PEG-b-PLA solution and sonicated. The final concentration of the PSi NPs was 100 μg mL^{-1}. The outer fluid was 0.2% of F127 in Milli-Q water adjusted to pH 12.8. Both fluids were pumped inside the microfluidic chip (10 and 100 mL h^{-1} for inner and outer fluids, respectively) and forced to coflow and mix rapidly inside the outer glass capillary, leading to the nanoprecipitation and formation of the PSi–PC (Figure 1). The empty compound micelles were obtained by the same experimental procedure used to produce PSi–PC NPs, but in this case PSi NPs were not included in the initial inner fluid.

Fabrication of the Glass-Capillary Microfluidic Hydrodynamic Flow Focusing Device: The microfluidic devices were made using a glass slide as a platform, to which borosilicate glass capillaries (World Precision Instruments, Inc.) were glued. Injection syringes (BD Luer-Lok syringe, 10 mL, and Terumo, 60cc Eccentric Luer Tip Syringe without Needle) and a pump (PHD 2000, Harvard Apparatus, USA) were used to introduce the flows to the channels at a constant flow rate. A borosilicate glass capillary with inner and outer diameters of 1100 and 1500 μm respectively was glued to a glass slide with transparent epoxy resin (5 min Epoxy, Devcon). Another borosilicate glass capillary, with inner and outer diameters of 560 and 1000 μm, respectively, was modeled using a micropipette puller (P-97, Sutter Instrument Co., USA) to a diameter of 10 μm, and was then enlarged to 100 μm manually using fine sandpaper. This capillary was inserted into the bigger capillary already glued to the glass slide and coaxially aligned with it. Then, the capillary was fixed with epoxy. The injection needles were glued to the entrance of the smaller glass capillary and to the entrance of the big glass capillary to the pump, respectively, with the inner and outer flows going through them.

Sorting and Lyophilization of PSi–PC: The PSi–PC NPs were concentrated to 200 μg mL^{-1} by centrifugation in filters with a membrane pore size of 100 kDa (Amicon Ultra; Merck Millipore Ltd.). Additionally, the NPs were lyophilized and stored at +4 °C. For this, the content of the filtering units was resuspended in a cryo-lyoprotectant, sucrose 0.5 M, frozen in liquid nitrogen for 24 h, and lyophilized (HETO LyoPro 3000, Heto/Holten A&S, Allerød, Denmark).

Characterization of the PSi–PC: The size distribution and polydispersity of the system was studied by multiangular DLS using a Brookhaven Instruments BI-200SM goniometer, a BIC-TurboCorr digital pseudocross-correlator, a BI-CrossCorr detector including two BIC-DS1 detectors. The Sapphire 488–100 CDRH laser from Coherent GmbH operating at $\lambda = 488$ nm and the power of 50 mW was used as a light source and the detector was set at different scattering angles, i.e., 45°, 60°, 90°, and 135°. The polydispersity was estimated using the second order cumulant fit and represents the size distribution width of the NPs' population.[16] Freshly prepared PSi–PC were suspended in Milli-Q water modified to pH around 7.4 to preserve the NPs' structure. Before the analysis, the PC and PSi–PC suspensions were diluted to 100 and 10 μg mL^{-1} and filtered using a 0.45 μm membrane pore size filter with PVDF membrane (Millipore) to remove dust. The surface chemistry of PSi and PSi–PC was studied with an FTIR (Vertex 70, Bruker, USA), equipped with a horizontal attenuated total reflectance accessory (Miracle, PIKE Technologies, USA). The FTIR spectra were registered using OPUS 5.5 software, from 4000–650 cm^{-1}, with a resolution of 4 cm^{-1}. The appearance of the self-assembled nanocomposite was visualized by TEM (Tecnai 12, FEI Company, USA) at an acceleration voltage of 120 kV. The sample was prepared by depositing 5 to 10 μL of the nanoparticles' suspension (20 μg $mL^{-1}$for PSi; 50 μg mL^{-1} for PSi–PC) on top of carbon-coated copper grids (300 mesh; Electron Microscopy Sciences, USA). Samples were let to settle down for 5 min prior to carefully removing the excess of liquid with filter paper. The sample was then washed twice with Milli-Q water and negatively stained for 1 min at room temperature with sterile-filtered uranyl acetate aqueous solution (2%, w/v), after which the sample was observed. TEM imaging was also used to study changes in PSi–PC toward media at different pH-values. PSi–PC samples were redispersed in Milli-Q water at pH 5.5 and 7.4 and gently stirred for 30 min. The samples were mounted and stained onto the carbon-coated copper grid following the above-mentioned procedure. The surface of bare PSi and PSi–PC was further observed using SEM (ZEISS Ultra-55 Scanning Electron Microscope). For the sample preparation the lyophilized product was redispersed in Milli-Q water at pH 7.4 and deposited on a Si wafer attached to a SEM sample holder. Then, the sample was dried under vacuum and sputter-coated with a 1 nm thick layer of PT:PD (80:20), prior to visualization by SEM.

Stability of the Nanocarriers in Human Plasma: The PSi and PSi–PC, were suspended in PBS (150 μL) and added to human plasma (1 mL) (obtained from anonymous donor from the Finnish Red Cross Blood Service) to a concentration of 150 μg mL^{-1}. The suspension was stirred under 37 °C, and samples were withdrawn after 1, 2, 5, 10, 20, 30, 60, 90, and 120 min. The samples were transferred and diluted into a folded capillary cell (Malvern Instruments) and the size, PDI, and ζ-potential were measured by DLS (Zetasizer Nano ZSP, Malvern Instruments, UK). Each experiment was performed at least in triplicate.

Particle Size and ζ-Potential at Different pH-Values: The pH sensitivity of the polymeric micelles was measured by adding PSi–PC (100 μg) to human plasma (1 mL) with the pH adjusted to different values (3, 5.5, 6.5, and 7.4) by adding 1 and 0.1 M HCl. All samples were stirred for 30 min and an aliquot was transferred to a disposable folded capillary cell (Malvern Instruments) and diluted. The sample was homogenized and measured (Zetasizer Nano ZSP, Malvern Instruments, UK). Each experiment was performed at least in triplicate. The size of the PSi–PC NPs was also evaluated by TEM. For this, the NPs (100 μg) were stirred for 30 min in buffer at pH 7.4, 6.8, and 5.5 (1 mL), before preparing the sample for TEM analysis.

Drug Loading and Loading Degree: Sorafenib (SFN) was loaded into the PSi NPs using the immersion method. The drug was dissolved in acetone (2 mg mL^{-1}) and PSi was added to the solution in a ratio of SFN:PSi of 6.7:1. The suspension was stirred for 90 min to allow the loading of the drug within the mesopores of PSi. After stirring, the suspension was centrifuged at 15 000 rpm for 5 min and the supernatant with excess of free drug was removed. Consequently, the particles were washed with 20% acetone in Milli-Q (500 μL) to remove the remaining free drug on the surface of the PSi NPs. The samples were centrifuged, the supernatant removed and the pellet resuspended in the medium of interest. The loaded PSi NPs were used to produce the nanocomposites, rendering the SFN-loaded nanocomposites. In order to calculate the loading degree of SFN in PSi, the NPs were resuspended with acetone (500 μL) and added to a vial containing acetone (1 mL) and stirred for 1.5 h to allow the complete release of the drug. Then the suspension was centrifuged at 15 000 rpm for 5 min and the supernatant (180 μL) was collected and analyzed by HPLC.

pH-Dependent Drug Release: The SFN-loaded PSi and SFN-loaded PSi–PC (300 μg) were added to PBS–FBS 10% at pH 5.5 and 6.8, and plasma at pH 7.4, (50 and 15 mL, respectively). SFN (200 μg) was added to PBS–FBS 10% pH 5.5 and plasma pH 7.4 (220 and 15 mL, respectively). The samples were stirred at 500 rpm and 37 °C. At each time point media (200 μL) was withdrawn for analysis and replaced with fresh media to keep the volume of dissolution constant. The samples were centrifuged at 15 000 rpm for 5 min, and 180 μL of the supernatant were transferred to a new Eppendorf tube. Acetone was added to the supernatant of PBS–FBS 10% and plasma (45 and 180 μL, respectively), vortexed for 30 s, and centrifuged in order to precipitate the proteins present in serum and plasma. The supernatant was collected and the concentration of SFN determined by HPLC.

Cell Culture: Human prostate cancer PC3MM2 cells (ATCC) were grown in a Dulbecco's modified Eagle's medium (DMEM) supplemented with 10% FBS, 1% nonessential amino acids (NEAA), and 1% penicillin/streptomycin (PEST); and incubated at 37 °C in a 5% CO_2 atmosphere. Cells were thawed from a frozen stock and passed until passage numbers between 30 and 40.

In Vitro Cytotoxicity: In vitro cytotoxicity was evaluated for the PSi NPs and PSi–PC. The NPs were incubated for 24 h with PC3MM2 cells at 37 °C and pH-values of 5.5 and 7.4. The NPs' suspensions were prepared at concentrations ranging from 50 to 1000 μg mL^{-1} based on the amount of PSi in both cases. PC3MM2 cells were seeded in a 96-well plate (1×10^5 cells mL^{-1}; 100 μL) and incubated overnight at 37 °C to allow the cells to attach. Then, the medium was removed and the wells were washed twice with 1× HBSS (pH 7.4). The particles used for these experiments were prepared at different concentrations in phenol-free DMEM supplemented with 10% FBS, 1% NEAA, and 1% PEST; and 100 μL of the suspensions were added to each well. After incubation, the cell viability was assessed with CellTiter-Glo Reagent (Promega Corporation, USA). Luminescence was measured with Varioskan Flash Fluorometer (Thermo Fisher Scientific, USA). All the experiments were performed at least in triplicate.

Growth Inhibition: Growth inhibition was tested at pH-values of 7.4 and 5.5, after 24 h incubation at 37 °C of the free drug SFN, and SFN-loaded PSi and PSi–PC NPs, in PC3MM2 cells. The concentrations of SFN used for the experiment varied from 0.02×10^{-6} to 120×10^{-6} M. The PC3MM2 cells were seeded in a 96-well plate (1×10^5 cells mL^{-1}; 100 μL per well) and incubated overnight at 37 °C to allow the cells to attach. Then, the medium was removed and the wells were washed twice with 1× HBSS (pH 7.4). The particles used for these experiments were prepared at different concentrations in phenol-free DMEM supplemented with 10% FBS, 1% NEAA, and 1% PEST; and 100 μL of the suspensions were added to each well. After incubation, the cell viability was assessed with CellTiter-Glo Reagent (Promega Corporation, USA). The luminescence was measured with Varioskan Flash Fluorometer (Thermo Fisher Scientific, USA). All the experiments were performed at least in triplicate.

In Vitro Macrophage-Mediated Phagocytosis of PSi and PSi–PC: The phagocytosis of the nanocomposites by RAW 264.7 macrophage cells was studied using confocal microscope and flow cytometry. In both cases, a negative control of RAW 264.7 cells without any treatment, as well as positive controls of RAW 264.7 cells treated with PSi and PSi–PC were performed. In the case of confocal microscopy, the cells were seeded in an 8-chamber slide (Nunc Lab-Tek II Chamber Slide System, Thermo scientific, Inc., USA) of 2.5×10^5 cells mL^{-1} (200 μL per chamber), and incubated overnight at 37 °C to allow the cells to attach prior to the addition of the fluorescently labeled NPs. PSi was labeled by loading with TRITC (Sigma-Aldrich, USA). Shortly, PSi NPs (400 μg) were stirred for 2 h with a TRITC solution (25 μL; 200 μg mL^{-1}) and washed twice with Milli-Q water (300 μL). Thereafter, PSi was either resuspended in phenol-free DMEM supplemented with 10% FBS, 1% NEAA, and 1% PEST to a concentration of 100 μg mL^{-1} or used to produce PSi–PC, as previously described, and resuspended in the same medium to a concentration of 100 μg mL^{-1}. Next, the prepared NPs' suspension (200 μL) was added to each chamber, and phenol-free DMEM supplemented with 10% FBS, 1% NEAA, and 1% PEST (200 μL) was added as the negative control. The samples were incubated for 24 h at 37 °C. Subsequently, the chambers were washed once with 1× HBSS (pH 7.4) and the cell membranes were stained using CellMask Deep Red (Life Technologies, USA) according to the manufacturer's instructions. Finally, the chambers were washed three times with 1× HBSS (pH 7.4) and the cells were fixed with 2.5% glutaraldehyde (Sigma-Aldrich, USA) for 15 min. The fixative was removed by rinsing the chambers three times with buffer and the samples were kept at 5 °C until their visualization by confocal microscope (Leica inverted confocal microscope SP5 II HCS A) provided by Ar (488 nm) and HeNe (633 nm) lasers, and a water immersion objective HCX PL APO 63×. For flow cytometry, the cells were seeded in a 6 well-plate (2.5×10^5 cells mL^{-1}; 2 mL per well) and incubated overnight at 37 °C to allow attachment to the bottom prior to putting the cells in contact with the fluorescently labeled NPs. PSi was covalently attached to Alexa Fluor 488 (AF; Life Technologies, USA) through an undecinyl acid linker. Briefly, the acidic groups from the undecinyl linker were activated to react with the dye through an *N*-ethyl-*N*′-(3-(dimethylamino)propyl) carbodiimide (EDC)/*N*-hydroxysuccinimide (NHS) reaction. The reactive PSi NPs were stirred for 3 h with AF in a ratio of 100:1 of the PSi to dye, and afterward washed twice with Milli-Q water (300 μL). As in the previous experiments, the PSi was either resuspended in phenol-free DMEM supplemented with 10% FBS, 1% NEAA, and 1% PEST to a concentration of 100 μg mL^{-1}, or used to produce PSi–PC and resuspended in the same medium to a concentration of 100 μg mL^{-1}. Consequently, AF-labeled nanocomposites were put in contact with the cells. For this, the wells were washed once with 1× HBSS (pH 7.4) and the AF-labeled PSi or AF-labeled PSi–PC (1 mL) were added to each well. For the negative control, phenol-free DMEM supplemented with 10% FBS, 1% NEAA, and 1% PEST (1 mL) was tested. Samples were incubated for 24 h at 37 °C, whereupon the medium was removed from the wells and the cells were harvested from the bottom of the wells, following the above-mentioned procedure. The cells were washed three times with 1× HBSS (pH 7.4) in order to remove the NPs not associated with the cells' membrane. With the aim of quenching the fluorescence coming from extracellular associated NPs, the cells were treated with Trypan Blue (0.005% v/v; 700 μL per 1×10^6 cells) for 5 min. Finally, the cells were washed three times with 1× HBSS (pH 7.4), suspended in this buffer (0.5 mL), and their fluorescence was quantified by flow cytometry (Galios Flow Cytometer; Beckman Coulter, Inc.; blue laser 488 nm). The data was post-processed using the software FlowJo X (FlowJo, LLC).

Statistical Analysis: Results are expressed as the mean ± standard deviation (s.d.) of at least three independent experiments. Statistical significance of the data was calculated from a one–way analysis of variance (ANOVA), followed by a Student's *t*-test with the level of significance set at a probability of $*p < 0.05$, $**p < 0.01$, and $***p < 0.001$ (GraphPad Prism 6.0e. GraphPad Software, Inc.).

Supporting Information

Supporting Information is available from the Wiley Online Library or from the author.

Acknowledgements

H.A.S. acknowledges financial support from the Academy of Finland (Decision Nos. 252215 and 256394), the University of Helsinki Research Funds, the Biocentrum Helsinki, and the European Research Council under the European Union's Seventh Framework Programme (FP/2007–2013, Grant No. 310892). H.Z. acknowledges Finnish Cultural Foundation for Postdoc Pooli grant. The authors thank the Electron Microscopy Unit and the Neuroscience Unit of the Institute of Biotechnology, University of Helsinki, for providing laboratory facilities for TEM imaging and FACS experiments, respectively. The authors thank Prof. David A. Weitz's lab at Harvard University for providing SEM facilities.

Received: November 20, 2014
Revised: January 7, 2015
Published online: January 22, 2015

[1] a) D. Peer, J. M. Karp, S. Hong, O. C. Farokhzad, R. Margalit, R. Langer, *Nat. Nanotechnol.* **2007**, *2*, 751; b) P. J. Kinnari, M. L. Hyvönen, E. M. Mäkilä, M. H. Kaasalainen, A. Rivinoja, J. J. Salonen, J. T. Hirvonen, P. M. Laakkonen, H. A. Santos, *Biomaterials* **2013**, *34*, 9134; c) T. Ji, Y. Zhao, Y. Ding, G. Nie, *Adv. Mater.* **2013**, *25*, 3508.

[2] a) B. Herranz-Blanco, L. R. Arriaga, E. Mäkilä, A. Correia, N. Shrestha, S. Mirza, D. A. Weitz, J. Salonen, J. Hirvonen, H. A. Santos, *Lab Chip* **2014**, *14*, 1083; b) H. Zhang, D. Liu, M. A. Shahbazi, E. Mäkilä, B. Herranz-Blanco, J. Salonen, J. Hirvonen, H. A. Santos, *Adv. Mater.* **2014**, *26*, 4497; c) F. Araújo, N. Shrestha, M.-A. Shahbazi, P. Fonte, E. M. Mäkilä, J. J. Salonen,

J. T. Hirvonen, P. L. Granja, H. A. Santos, B. Sarmento, *Biomaterials* **2014**, *15*, 609; d) C.-F. Wang, E. M. Mäkilä, M. H. Kaasalainen, D. Liu, M. P. Sarparanta, A. J. Airaksinen, J. J. Salonen, J. T. Hirvonen, H. A. Santos, *Biomaterials* **2014**, *35*, 1257; e) N. Shrestha, M.-A. Shahbazi, F. Araújo, H. Zhang, E. M. Mäkilä, J. Kauppila, B. Sarmento, J. J. Salonen, J. T. Hirvonen, H. A. Santos, *Biomaterials* **2014**, *35*, 9199; f) D. Liu, H. Zhang, B. Herranz-Blanco, E. Mäkilä, V. P. Lehto, J. Salonen, J. Hirvonen, H. A. Santos, *Small* **2014**, *10*, 2029.

[3] a) N. Vale, E. Mäkilä, J. Salonen, P. Gomes, J. Hirvonen, H. A. Santos, *Eur. J. Pharm. Biopharm.* **2012**, *81*, 314; b) M. Tahvanainen, T. Rotko, E. Mäkilä, H. A Santos, D. Neves, T. Laaksonen, A. Kallonen, K. Hämäläinen, M. Peura, R. Serimaa, *Int. J. Pharm*. **2012**, *422*, 125.

[4] a) H. A. Santos, L. M. Bimbo, V.-P. Lehto, A. J. Airaksinen, J. Salonen, J. Hirvonen, *Curr. Drug Discovery Technol.* **2011**, *8*, 228; b) J. Salonen, V.-P. Lehto, *Chem. Eng. J.* **2008**, *137*, 162.

[5] D. Liu, B. Herranz-Blanco, E. Mäkilä, L. R. Arriaga, S. Mirza, D. A. Weitz, N. Sandler, J. Salonen, J. Hirvonen, H. A. Santos, *ACS Appl. Mater. Interfaces* **2013**, *5*, 12127.

[6] a) S. S. Rao, N. Han, J. O. Winter, *J. Biomater. Sci.* **2011**, *22*, 611; b) M. Hoque, D. Hutmacher, W. Feng, S. Li, M.-H. Huang, M. Vert, Y. Wong, *J. Biomater. Sci.* **2005**, *16*, 1595.

[7] E. S. Lee, H. J. Shin, K. Na, Y. H. Bae, *J. Controlled Release* **2003**, *90*, 363.

[8] H. Yin, E. S. Lee, D. Kim, K. H. Lee, K. T. Oh, Y. H. Bae, *J. Controlled Release* **2008**, *126*, 130.

[9] K. Park, *Biomaterials for Cancer Therapeutics: Diagnosis, Prevention and Therapy*, Woodhead Publishing, Cambridge, UK **2013**.

[10] a) N. Kolishetti, S. Dhar, P. M. Valencia, L. Q. Lin, R. Karnik, S. J. Lippard, R. Langer, O. C. Farokhzad, *Proc. Natl. Acad. Sci. U.S.A.* **2010**, *107*, 17939; b) R. Karnik, F. Gu, P. Basto, C. Cannizzaro, L. Dean, W. Kyei-Manu, R. Langer, O. C. Farokhzad, *Nano Lett.* **2008**, *8*, 2906.

[11] L. Zhang, A. Eisenberg, *J. Am. Chem. Soc.* **1996**, *118*, 3168.

[12] H. Deng, Y. Zhong, M. Du, Q. Liu, Z. Fan, F. Dai, X. Zhang, *Theranostics* **2014**, *4*, 904.

[13] M. Stubbs, P. M. McSheehy, J. R. Griffiths, C. L. Bashford, *Mol. Med. Today* **2000**, *6*, 15.

[14] a) A. N. Koo, K. H. Min, H. J. Lee, S.-U. Lee, K. Kim, I. Chan Kwon, S. H. Cho, S. Y. Jeong, S. C. Lee, *Biomaterials* **2012**, *33*, 1489; b) J. A. Barreto, W. O'Malley, M. Kubeil, B. Graham, H. Stephan, L. Spiccia, *Adv. Mater.* **2011**, *23*, H18.

[15] E. D. Hugger, K. L. Audus, R. T. Borchardt, *J. Pharm. Sci.* **2002**, *91*, 1980.

[16] W. Schärtl, *Light Scattering from Polymer Solutions and Nanoparticle Dispersions: With 16 Tables*, Springer, Berlin Heidelberg **2007**.

[17] a) M.-A. Shahbazi, T. D. Fernández, E. M. Mäkilä, X. Le Guével, C. Mayorga, M. H. Kaasalainen, J. J. Salonen, J. T. Hirvonen, H. A. Santos, *Biomaterials* **2014**, *35*, 9224; b) P. V. Almeida, M.-A. Shahbazi, E. Mäkilä, M. Kaasalainen, J. Salonen, J. Hirvonen, H. A. Santos, *Nanoscale* **2014**, *6*, 10377.

[18] a) D. E. Owens III, N. A. Peppas, *Int. J Pharm.* **2006**, *307*, 93; b) C. Röcker, M. Pötzl, F. Zhang, W. J. Parak, G. U. Nienhaus, *Nat. Nanotechnol.* **2009**, *4*, 577; c) S. Tenzer, D. Docter, J. Kuharev, A. Musyanovych, V. Fetz, R. Hecht, F. Schlenk, D. Fischer, K. Kiouptsi, C. Reinhardt, K. Landfester, H. Schild, M. Maskos, S. K. Knauer, R. H. Stauber, *Nat. Nanotechnol.* **2013**, *8*, 772.

[19] a) H. Wu, L. Zhu, V. P. Torchilin, *Biomaterials* **2013**, *34*, 1213; b) E. S. Lee, K. Na, Y. H. Bae, *Nano Lett.* **2005**, *5*, 325.

[20] M. Sarparanta, L. M. Bimbo, J. Rytkönen, E. Mäkilä, T. J. Laaksonen, P. Laaksonen, M. Nyman, J. Salonen, M. B. Linder, J. Hirvonen, H. A. Santos, A. J. Airaksinen, *Mol. Pharmaceutics* **2012**, *9*, 654.

[21] H. A. Santos, J. Riikonen, J. Salonen, T. Heikkilä, E. Mälkiä, T. Laaksonen, L. Peltonen, V.-P. Lehto, J. Hirvonen, *Acta Biomater.* **2010**, *6*, 2721.

[22] R. Grefa, M. Lückb, P. Quellecc, M. Marchandd, E. Dellacheriec, S. Harnischb, T. Blunke, R. H. Müllerb, *Colloids Surf. B* **2000**, *18*, 301.

[23] L. M. Bimbo, M. Sarparanta, H. A. Santos, A. J. Airaksinen, E. Mäkilä, T. Laaksonen, L. Peltonen, V.-P. Lehto, J. Hirvonen, J. Salonen, *ACS Nano* **2010**, *4*, 3023.